

# rf measurements and tuning of the 750 MHz radio frequency quadrupole

Benjamin Koubek,<sup>\*</sup> Alexej Grudiev,<sup>†</sup> and Marc Timmins<sup>‡</sup>

CERN, CH-1211 Geneva-23, Switzerland

(Received 18 April 2017; published 9 August 2017)

In the framework of the program on medical applications a compact 750 MHz RFQ has been designed and built to be used as an injector for a hadron therapy linac. This RFQ was designed to accelerate protons to an energy of 5 MeV within only 2 m length. It is divided into four segments and equipped with 32 tuners in total. The length of the RFQ corresponds to  $5\lambda$  which is considered to be close to the limit for field adjustment using only piston tuners. Moreover the high frequency, which is about double the frequency of existing RFQs, results in a sensitive structure and requires careful tuning. In this paper we present the tuning algorithm, the tuning procedure and rf measurements of the RFQ.

DOI: 10.1103/PhysRevAccelBeams.20.080102

## I. INTRODUCTION

The high frequency RFQ (HF-RFQ), shown in Fig. 1, for medical applications will be used as an injector for the LIGHT project, a linac based proton therapy facility [1,2]. Beam dynamics parameters have been chosen in order to minimise beam losses above 1 MeV and to meet the requirements as an injector for facilities working at 3 GHz [3]. From an RF point of view the very compact 750 MHz 4-vane structure operates at about twice the frequency of existing RFQs [4], increasing the demand of mechanical precision. It consists of four modules with a length of about half a meter. The parameters of the RFQ are summarized in Table I.

In order to meet the required beam and rf parameters a RFQ needs to be precisely machined and assembled but also properly set up in terms of rf parameters. The field tuning plays an important role in order to deliver the longitudinal voltage distribution as required from the beam dynamics design. This means in our case a constant longitudinal distribution of the quadrupole mode. The influence of dipole modes should be as small as possible.

The tuning of a 4-vane RFQ is usually done by moving an array of piston tuners that influence the fields inside the cavity. In order to perform the field tuning a relation needs to be made between the desired and measured fields of the cavity and the dimensions of the tuners. In general many tuner algorithms for accelerator cavities are based on equivalent circuit models [5–7]. This is also the case for RFQs, where the measurable field errors, usually obtained

using the standard bead-pulling technique, are described as elements of the circuit [8–10]. Then different mathematic approaches can be used to find tuner settings that adjust the fields to the desired values [11–13]. Usually after a few iterations a satisfactory field distribution is reached. In our approach the influence of the tuners was measured directly to obtain a response matrix that describes the relation between actual and desired fields and the tuner settings. Problems like inverting a nonsquare and ill-conditioned matrix in this case have been solved by using singular values decomposition (SVD) of the matrix as discussed in this paper. This leads to a simple and powerful tuning algorithm that allowed a fast field tuning of the RFQ.

Also the high frequency of the RFQ lead to a demand of high precision in terms of tuner placement. Often dummy tuners are used for field adjustment and final tuners are machined according to measurements [14,15]. In our case a tuner tooling was developed to allow us to directly adjust the position of the final tuners.



FIG. 1. The picture shows the fully assembled RFQ while tuning and bead pull measurements were made with the attached power couplers, pumping ports and tuners. The tuners are mounted with a tuner tooling that allowed a precise adjustment of the tuners penetration depth for tuning.

<sup>\*</sup>benjamin.koubek@cern.ch

<sup>†</sup>alexej.grudiev@cern.ch

<sup>‡</sup>marc.timmins@cern.ch

Published by the American Physical Society under the terms of the *Creative Commons Attribution 4.0 International license*. Further distribution of this work must maintain attribution to the author(s) and the published article's title, journal citation, and DOI.

TABLE I. Main RFQ parameters.

Parameter	Value
Input/Output Energy	40 keV/5 MeV
Length	1.964 m
Vane voltage	67.6 kV
Min aperture radius	1 mm
$R_0$	2 mm
$\rho$	1.5 mm
Maximum modulation	3
Final synchronous phase	-15 deg
Output Pulse Current	30 $\mu$ A
Beam transmission	30%
Output transv. rms emit.	0.027 $\pi$ mm mrad
Output phase spread	$\pm 2$ deg
Output energy spread	$\pm 20$ keV
RF Frequency	750 MHz
RF Power	350 kW
Operation Duty Cycle	0.4%

The paper will describe the measurement equipment and the tuner tooling that was specifically developed for this RFQ. Measurements on single modules are presented and compared to simulations. The tuning algorithm will be introduced and explain how SVD (singular value decomposition) was used to invert the nonsquare and ill-conditioned response matrix. This is followed by a description of the tuning procedure paying special attention to the use of different obtained solutions for tuner settings by the algorithm in order to avoid remeasuring the response matrix and to speed up the tuning process.

## II. MEASUREMENT EQUIPMENT

### A. Bead pull system

The bead pull system, meaning all parts necessary to make the bead travel through all the quadrants of the HF-RFQ, was previously used for the tuning of the LINAC4 RFQ at CERN [16,17]. All the components were reused for the newly built RFQ and adapted onto a cradle support separately built unlike the LINAC4 system which saw the components directly attached to the RFQ. The pulleys, adjustment devices and motor were assembled in a way to fit the RFQs dimensions. Pictures in Fig. 2 show the bead pull setup.

An aluminum bead with a length of 7 mm and a diameter of 4 mm was used to gain proper bead pull results. A smooth movement of the bead through the 4 quadrants and around all pulleys was achieved by using a 0.3 mm fishing wire.

### B. Tuner tooling

In order to achieve an accurate adjustment of the position of the tuner a special tool was developed. Figure 3 shows cross-sectional views of this tuner tool.



FIG. 2. The picture shows the bead pull measurements setup of the fully assembled RFQ in the laboratory including equipment like VNA (vector network analyser) and power supply for the motor that drives the wire.

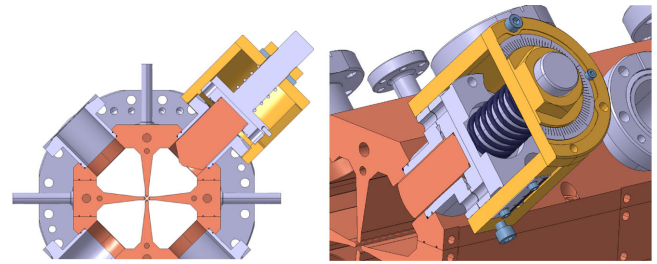


FIG. 3. Cross sections of the tuner tooling. The drawing shows the tuner itself, the mounted thread for adjustment of the penetration depth and the tube that attaches the tuner tooling to the flange.

The tuner itself slides along a tube attached to the outer surface of the tuning port flange which offers an accurate transversal position. With the help of a fine thread screw attached to the back of the tuner and a lateral pin preventing its rotation the tuner slides along the tooling tube with a pitch of 1 mm per turn given to the nut on the outer side. The play in the thread is suppressed with the help of a



FIG. 4. The picture shows the coarse and fine scaling of the tuner tooling to adjust the penetration depth of the a tuner. The nut on the left side was used to vary the penetration depth of the tuner.

spring providing continuous contact to one side of the thread. For alignment a coarse scaling with 1 mm steps using the pin as reference was provided, while a finer scaling on the screw-nut with 1/100 mm division was used for precise alignment. Two pictures of the scaling at the tuner tooling is shown in Fig. 4.

### III. SINGLE MODULE MEASUREMENTS

Measurements on single modules have been made in order to compare the longitudinal field distribution to simulation results and assess if there is any need for the use of the pumping ports as tuning features in addition to the tuners. Besides this the single modules were used to debug and align the bead pull system to guarantee preparation for the full assembly measurements.

To match the boundary conditions two extension parts were attached to the modules. These parts, shown in Fig. 5, are tubes that were adjusted in length and diameter by simulations to allow the field to decay within the tube. The diameter was matched to meet the frequency of the RFQ. Since the fringe fields of the RFQ decay exponentially with

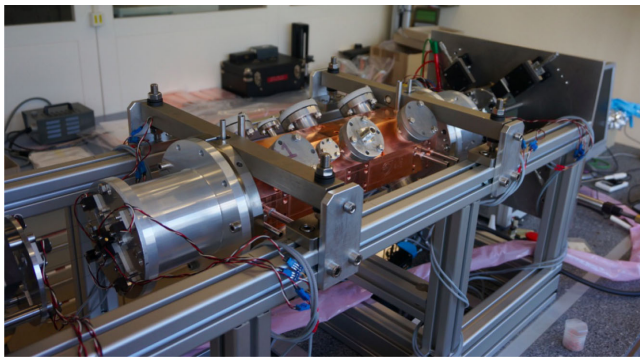


FIG. 5. The picture shows the extension parts, made of aluminum, attached to the extremities of a single module. These parts provide comparable boundary conditions to simulations.

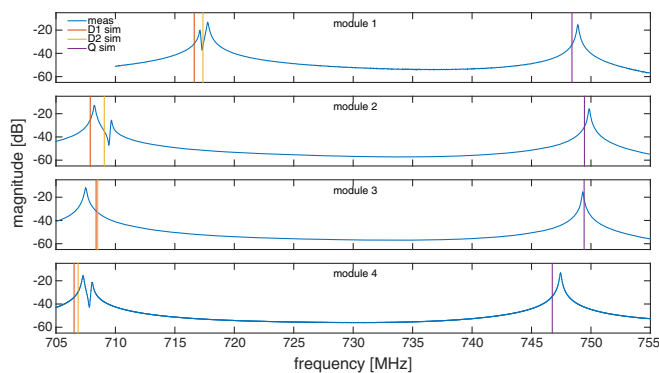


FIG. 6. Comparison of measurements (blue) and simulations of the frequency of the first three modes of the four single modules.

distance, the length of the tube was chosen to be as long as the frequency did not depend on the tube length anymore.

The bead pull and mode spectra measurements of the single modules have been compared to simulation results in order to assess the mechanical accuracy of the single modules. In Fig. 6 the first two dipole modes  $TE_{110}$ ,  $TE_{111}$  and the operating quadrupole mode  $TE_{210}$  of all modules are

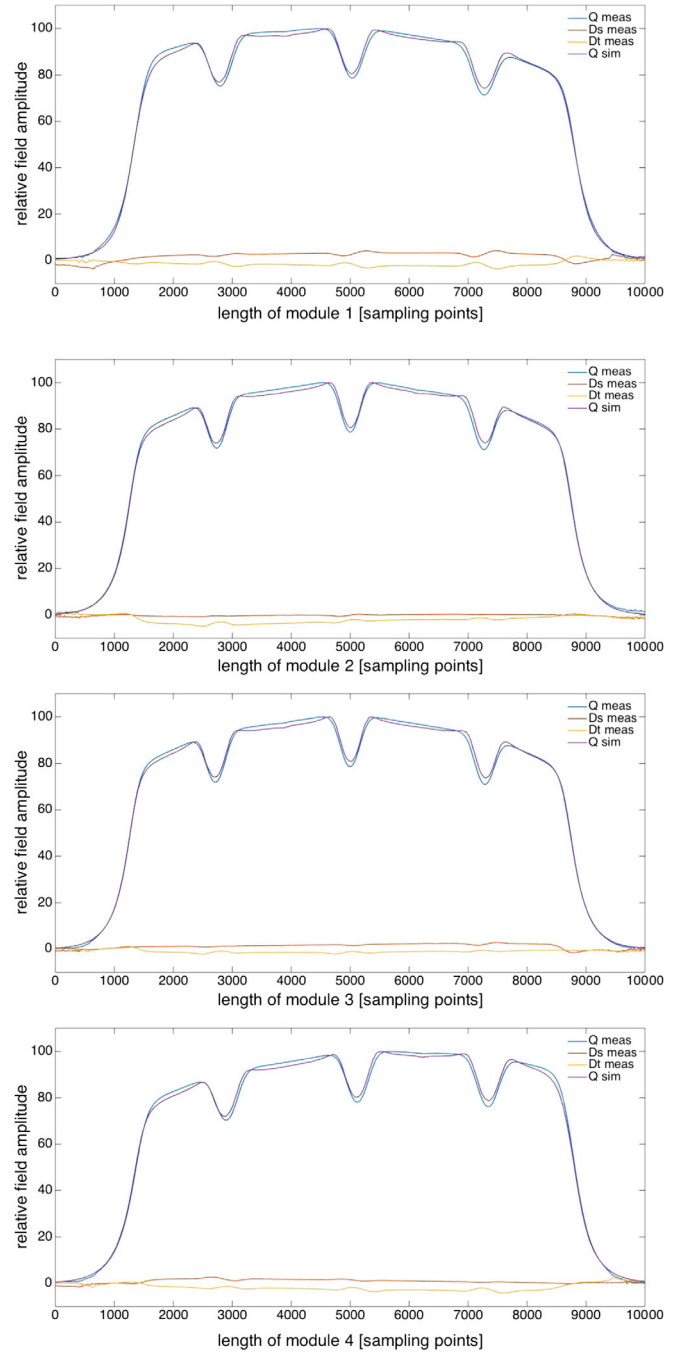


FIG. 7. From top to bottom module 1 to 4. The plots show the comparison of measured Q, Ds and Dt components with simulation of the Q component. In simulations the Ds and Dt vanish completely.

TABLE II. Errors of the Ds and Dt components of the single modules.

Module	Error Ds	Error Dt
1	$\pm 2.8\%$	$\pm 2.8\%$
2	$\pm 0.5\%$	$\pm 2.8\%$
3	$\pm 2.2\%$	$\pm 1.7\%$
4	$\pm 1.4\%$	$\pm 2.4\%$

shown. The measured spectra is the blue line and the cursors indicate the values from simulations. The agreement of the values from simulations and the measured values are within a 0.7 MHz range. Since the dipole modes are strongly length dependent this does not represent this difference between dipole and quadrupole modes of the full assembly of the RFQ, it was used to compare measurements with simulations.

In Fig. 7 the Q, Ds and Dt components of the single modules are compared to simulations at the actual frequency of the  $TE_{210}$  mode of the modules. Since the dipole components of the  $TE_{210}$  mode is zero in simulations it is not included in the plots. The Q component shows a very good agreement between measurement and simulation for all modules. The difference is below the effect of the displacement of the wire in one quadrant of 1 mm. The errors of the dipolar components, Ds and Dt, of the single modules are all within  $\pm 3\%$ . This confirms the precise machining and brazing within the specified tolerances. A comparison of all dipolar components of the single modules is given in Table II.

The errors of modules 1 and 4 might also be attributed to the more complex geometry of the modules with the vane undercuts at the extremities of the RFQ. Maximum errors for the quadrupole components are about  $\pm 2.6\%$  by means of local deviations from simulations.

#### IV. FULL ASSEMBLY OF THE RFQ

The high frequency of the RFQ leads to a high demand on machining and assembly tolerances as well as for field errors. Machining tolerances based on error studies of mechanical errors, rf jitter and beam errors were  $\pm 10 \mu\text{m}$  for the cavity and  $\pm 5 \mu\text{m}$  for the vane tips. The assembly tolerance for the four vanes was  $\pm 15 \mu\text{m}$  [4]. From the finally reached machining and alignment errors field errors of  $\pm 2\%$  for Q, Ds and Dt could be tolerated by beam dynamics. The tuning range spanned by the tuners was  $\pm 11 \text{ mm}$  that corresponds to a total frequency shift of  $\pm 13.73 \text{ MHz}$ . However during the tuning less than half of the tuner range ( $\pm 4.2 \text{ mm}$ ) was needed to reduce field errors below  $\pm 2\%$ . A measured mode spectra of the fully assembled RFQ is shown in Fig. 8, where the operating mode is indicated with  $Q_0$ . The plot shows a separation of the neighboring dipolar modes by more than 10 MHz after

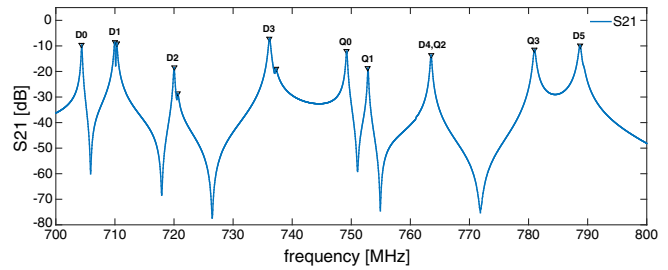


FIG. 8. Measurement of Mode spectra of the fully assembled RFQ. The different dipole (D) and quadrupole (Q) modes are indicated.

full assembly of the RFQ including the end flanges with dipole stabilizer rods.

#### A. Reliability tests

Before the tuning process was started, several tuner movements were executed in order to learn about mechanical hysteresis effects of the tuner tooling and to determine reliability of the placements of the single tuners. An improved handling of the tuner tooling guaranteed a reliable tuner movement in a way such that a certain penetration depth of a tuner always gives the same results for frequency and field distribution.

A bead pull measurement of all quadrants and calculation of the Q, Ds and Dt components was done for the movement of tuner 6 and tuner 25. A tuner in first and fourth module was chosen in order to estimate the possible field tuning range. Figure 9 shows a plot of all components of the movements of the two tuners.

The quadrupole component could be compensated almost using only one tuner. From this plot it is also obvious that to compensate also the dipole components at the same time a more complex tuner configuration is necessary. The sensitivity of the tuners is well within the range of the initial field distribution.

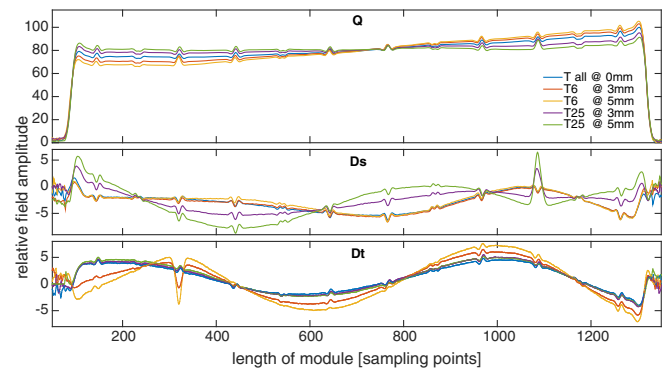


FIG. 9. The plot shows the development of the measured relative longitudinal field distribution by moving the tuners T6 and T25 inside by 3 mm and 5 mm respectively. The maximal initial field of Q is normalised to 100%.

This plot also shows that tuner 6 in quadrant  $q2$  has almost no influence on the Ds component that is calculated using quadrants  $q1$  and  $q3$ . The same behavior was found for tuner 25 in quadrant  $q1$  that does only barely affect the Dt component calculated using  $q2$  and  $q4$ .

### B. Tuning algorithm

The aim of tuning is to adjust the fields of the RFQ according to the requirements of the beam dynamics design. Therefore the RFQ is equipped with 32 tuners that can be moved precisely into the cavity to influence the fields. By adjusting the penetration depth of the tuners the magnetic field distribution in azimuthal and longitudinal direction can be influenced. The goal of the tuning process is to find a mechanical setting for each tuner that provides a constant longitudinal field distribution for the quadrupole mode (Q). The dipolar components (Ds, Dt) should be zero or minimised to a small fraction of the quadrupole component.

#### 1. Response matrix

The tuning algorithm is based on a response matrix that describes the influence of every tuner to every field component for all longitudinal locations. To obtain the field distribution the standard bead pull technique is used. The magnetic field distribution is described in terms of quadrupole (Q) and dipole (Ds, Dt) components. If  $q_1, \dots, q_4$  are the bead pull measurements of the longitudinal field distribution of the four quadrants, the transversal amplitudes are defined as

$$Q = (q_1 - q_2 + q_3 - q_4)/4 \quad (1)$$

$$Ds = (q_1 - q_3)/2 \quad (2)$$

$$Dt = (q_2 - q_4)/2 \quad (3)$$

The amplitudes are supposed to be

$$Q = \text{const.} \quad (4)$$

$$Ds = Dt = 0. \quad (5)$$

This implies that the magnetic flux in all quadrants is the same for a pure quadrupole mode. In longitudinal direction the quadrupole mode should be constant for the HF-RFQ and the dipole components should be as small as possible to guarantee a clean quadrupole mode. The field along the RFQ is determined by  $i$  measurement locations. As tuning devices we have a number of  $j$  tuners available. Then we define

$$\vec{V}_i = \vec{V}_{ii} - \vec{V}_{0i} \quad (6)$$

$$\vec{T}_j = \vec{T}_{ij} - \vec{T}_{0j} \quad (7)$$

where  $\vec{V}_i$  describes the difference between the target  $\vec{V}_{ii}$  and actual  $\vec{V}_{0i}$  longitudinal field distribution. The vector entries are the amplitudes of the Q, Ds and Dt components obtained from measurements. The vector  $\vec{T}_j$  is defined as the difference between the target  $\vec{T}_{ij}$  and actual  $\vec{T}_{0j}$  tuner setting of all tuners.

If we move one tuner a changed field distribution from the initial one can be measured. From this we can calculate the  $\partial \vec{V}_i$  and we know the change of tuner setting  $\partial \vec{T}_j$ . Now we can calculate the derivative of every field component for all longitudinal measurement locations  $\partial \vec{V}_i / \partial \vec{T}_j$ . If we do this for every single tuner one by one we can obtain a matrix that describes the influence of every tuner movement on all field components at all longitudinal positions and we can write the equation

$$\begin{bmatrix} 100 - V_1 \\ \vdots \\ 100 - V_{11} \\ 0 - V_{12} \\ \vdots \\ 0 - V_{22} \\ 0 - V_{23} \\ \vdots \\ 0 - V_{33} \end{bmatrix} = \begin{bmatrix} \frac{\partial Q_1}{\partial T_1} & \frac{\partial Q_1}{\partial T_2} & \dots & \dots & \frac{\partial Q_1}{\partial T_{32}} \\ \vdots & \vdots & \ddots & \ddots & \vdots \\ \frac{\partial Q_{11}}{\partial T_1} & \frac{\partial Q_{11}}{\partial T_2} & \dots & \dots & \frac{\partial Q_{11}}{\partial T_{32}} \\ \frac{\partial Ds_1}{\partial T_1} & \frac{\partial Ds_1}{\partial T_2} & \dots & \dots & \frac{\partial Ds_1}{\partial T_{32}} \\ \vdots & \vdots & \ddots & \ddots & \vdots \\ \frac{\partial Ds_{11}}{\partial T_1} & \frac{\partial Ds_{11}}{\partial T_2} & \dots & \dots & \frac{\partial Ds_{11}}{\partial T_{32}} \\ \frac{\partial Dt_1}{\partial T_1} & \frac{\partial Dt_1}{\partial T_2} & \dots & \dots & \frac{\partial Dt_1}{\partial T_{32}} \\ \vdots & \vdots & \ddots & \ddots & \vdots \\ \frac{\partial Dt_{11}}{\partial T_1} & \frac{\partial Dt_{11}}{\partial T_2} & \dots & \dots & \frac{\partial Dt_{11}}{\partial T_{32}} \end{bmatrix} \cdot \begin{bmatrix} T_1 - 0 \\ T_2 - 0 \\ \vdots \\ \vdots \\ \vdots \\ \vdots \\ \vdots \\ \vdots \\ T_{32} - 0 \end{bmatrix}$$

with the colored components Q (blue), Ds (red), and Dt (yellow). All colored entries are known by measurements and calculations. In short we can write

$$\vec{V} = \mathbf{M} \cdot \vec{T}. \quad (8)$$

The initial tuner setting is zero for all tuners and the only unknown is the tuner setting obtained by inverting the Matrix  $\mathbf{M}$ .

$$\vec{T} = \mathbf{M}^{-1} \cdot \vec{V}. \quad (9)$$

Due to errors in the tuner adjustment and the fact that the tuner movement does not influence field and frequency in a perfectly linear manner the procedure has to be repeated several times. Hence obtaining the desired field distribution is an iterative process. Therefore the calculated tuner settings  $\vec{T}_j$  has to be applied to the tuners and the field has to be remeasured to obtain a new  $\vec{V}_0$ . This has to be repeated until an acceptable difference in  $\vec{V}_{ii} - \vec{V}_{0i}$  is achieved [18].

The dimensions of the matrix are given by the number of tuners and by the number of measurement locations times three for three components Q, Ds, and Dt. For the HF-RFQ this was a  $32 \times 33$  nonsquare matrix and hence not very

simple to invert. In order to solve this the matrix was inverted using the singular value decomposition.

## 2. Singular value decomposition

An introduction how the singular value decomposition (SVD) was used for the tuning algorithm is given in the following. More detailed information about SVD can be found for example in Ref. [19]. A singular value decomposition is a factorization of normal or complex matrix into three matrices.

$$\mathbf{M} = \mathbf{USV}^T. \quad (10)$$

$\mathbf{U}$  is a  $m \times m$  and column orthogonal matrix whose columns are the eigenvectors of the  $\mathbf{MM}^T$  matrix (left eigenvectors)

$\mathbf{S}$  is a  $m \times n$  diagonal matrix whose diagonal elements (non-negative real values) are the singular values of  $\mathbf{M}$

$\mathbf{V}$  is a  $n \times n$  orthogonal matrix whose columns are the eigenvectors of the  $\mathbf{M}^T\mathbf{M}$  matrix (right eigenvectors)

$$\begin{bmatrix} \cdot & \cdot & \cdot \\ \cdot & \cdot & \cdot \\ \cdot & M & \cdot \\ \cdot & \cdot & \cdot \\ \cdot & \cdot & \cdot \end{bmatrix} = \begin{bmatrix} \cdot & \cdot & \cdot & \cdot \\ \cdot & \cdot & \cdot & \cdot \\ \cdot & \cdot & U & \cdot \\ \cdot & \cdot & \cdot & \cdot \\ \cdot & \cdot & \cdot & \cdot \end{bmatrix} \begin{bmatrix} \sigma_1 \\ \sigma_2 \\ \sigma_3 \\ \cdot \\ \cdot \end{bmatrix} \begin{bmatrix} \cdot & \cdot & \cdot \\ \cdot & V^T & \cdot \\ \cdot & \cdot & \cdot \end{bmatrix}$$

$\mathbf{S} = \text{diag}(\sigma_1, \sigma_2, \dots, \sigma_n)$  is ordered so that  $\sigma_1 \geq \sigma_2 \geq \dots \geq \sigma_n$  (if  $\sigma$  is an singular value of  $\mathbf{M}$  it's square is an eigenvalue of  $\mathbf{M}^T\mathbf{M}$ )

Besides other applications SVD is a powerful tool to compute the inverse of a matrix, even if it is nonsquare and ill-conditioned.

If  $\mathbf{M}$  is a  $n \times n$  matrix, its inverse is given by

$$\mathbf{M}^{-1} = \mathbf{VS}^{-1}\mathbf{U}^T \quad (11)$$

$$\text{where } \mathbf{S}^{-1} = \text{diag}\left(\frac{1}{\sigma_1}, \frac{1}{\sigma_2}, \dots, \frac{1}{\sigma_n}\right). \quad (12)$$

If  $\mathbf{M}$  is singular or ill-conditioned, SVD can be used to approximate its inverse by the following

$$\mathbf{M}^{-1} = (\mathbf{USV}^T)^{-1} \approx \mathbf{VS}_0^{-1}\mathbf{U}^T \quad (13)$$

$$\mathbf{S}_0^{-1} = \begin{cases} 1/\sigma_i & \text{if } \sigma_i > t \\ 0 & \text{otherwise} \end{cases} \quad (14)$$

where  $t$  is a small threshold.

If  $\mathbf{M}$  is a square matrix also  $\mathbf{S}$  is square and can be simple inverted by inverting each element of the matrix. If  $\mathbf{M}$  is nonsquare the also nonsquare diagonal matrix  $\mathbf{S}$  can be

inverted by using the pseudoinverse, inverting each element and then transposing it.

For the tuning process the following equation has to be solved.

$$\vec{V} = \mathbf{M} \cdot \vec{T}. \quad (15)$$

A solution of tuner settings is given by

$$\vec{T} = \mathbf{M}^{-1} \cdot \vec{V} \quad (16)$$

since this set of equations is overdetermined,  $\mathbf{M}$  is non-square and ill-conditioned and SVD is used for the inversion of  $\mathbf{M}$  and the pseudoinverse is used to obtain  $\mathbf{S}_0^{-1}$ . But still the solutions for  $\mathbf{T}$  might give some strange results. To solve this  $\mathbf{M}^{-1}$  is approximated by changing the threshold  $t$  for  $\mathbf{S}_0^{-1}$  as given in Eq. (14). To do so in a first step the largest  $1/\sigma_i$  is set to zero.

From now on the pseudoinverse of  $\mathbf{S}$  is named  $\mathbf{S}_{\text{inv}0}$  leading to a solution for a tuner setting

$$\vec{T}_{\text{svd}0} = (\mathbf{V} \cdot \mathbf{S}_{\text{inv}0} \cdot \mathbf{U}^T) \cdot \vec{V}. \quad (17)$$

Since  $\mathbf{M}$  is a  $33 \times 32$  matrix the number of singular values is 32. As first step to obtain an approximation for  $\mathbf{S}_0^{-1}$ ,  $\mathbf{S}_{\text{inv}1}$  is calculated by setting the largest inverse singular value to zero [Eq. (18)]. In a second step the second largest inverse singular value is set to zero [Eq. (19)], and so on.

$$1/\sigma_{32} = 0 \Rightarrow \mathbf{S}_{\text{inv}1} \quad (18)$$

$$1/\sigma_{31} = 0 \Rightarrow \mathbf{S}_{\text{inv}2} \quad (19)$$

⋮

$$1/\sigma_1 = 0 \Rightarrow \mathbf{S}_{\text{inv}32} \quad (20)$$

From these different  $\mathbf{S}_{\text{inv}i}$  also different tuner settings can be obtained using Eq. (17).

$$\vec{T}_{\text{svd}1} = (\mathbf{V} \cdot \mathbf{S}_{\text{inv}1} \cdot \mathbf{U}^T) \cdot \vec{V} \quad (21)$$

$$\vec{T}_{\text{svd}2} = (\mathbf{V} \cdot \mathbf{S}_{\text{inv}2} \cdot \mathbf{U}^T) \cdot \vec{V} \quad (22)$$

⋮

$$\vec{T}_{\text{svd}32} = (\mathbf{V} \cdot \mathbf{S}_{\text{inv}32} \cdot \mathbf{U}^T) \cdot \vec{V}. \quad (23)$$

Now we found 32 possible solutions for tuner settings to compensate  $\vec{V}$  in the first iteration. But some of these solutions can not be used due to large tuner settings that are clearly out of the mechanical tuning range. Also the different  $\mathbf{S}_{\text{inv}i}$  with manipulated singular values are only

approximations of  $\mathbf{S}_0^{-1}$  and one has to check the agreement of  $\vec{V}$ . These agreements are also an indication for how good a certain solution for  $\vec{T}_{svdi}$  might compensate the field derivation  $\vec{V}$ . These predictions are obtained by using the tuner settings  $\vec{T}_{svdi}$  and the original response matrix  $\mathbf{M}$ .

$$\vec{V}_{svd1} = \mathbf{M} \cdot \vec{T}_{svd1} \quad (24)$$

$$\vec{V}_{svd2} = \mathbf{M} \cdot \vec{T}_{svd2} \quad (25)$$

$$\vdots$$

$$\vec{V}_{svd32} = \mathbf{M} \cdot \vec{T}_{svd32}. \quad (26)$$

These predictions of which field deviation will be compensated  $\vec{V}_{svdi}$  can be compared to actual field deviation  $\vec{V}$  to find a best fitting tuner setting  $\vec{T}_{svdi}$  as shown in Fig. 10 on the top three plots. The graph shows the field that has to be compensated as blue dotted line. The other curves are a selection of different  $\vec{V}_{svdi}$  for different thresholds for the modification of the singular values. The plot on the bottom shows the corresponding  $\vec{T}_{svdi}$  to the  $\vec{V}_{svdi}$  above.

This figure shows that many of the tuner setting would lead to a quite good compensation of the quadrupole component (Q). For the dipole components (Ds and Dt) the deviation is much larger for some curves. The plot also shows only a selection of  $\vec{V}_{svd17}$  to  $\vec{V}_{svd26}$ . The other solutions are not very practical due to the large tuner settings in the range of up to 100 mm as well as poor agreement with  $\vec{V}$ . Solutions roughly for  $\vec{V}_{svd1}$  to  $\vec{V}_{svd15}$  show a good agreement in  $\vec{V}$  but too large tuner movement, while solutions for roughly  $\vec{V}_{svd25}$  to  $\vec{V}_{svd32}$  are in a reasonable range for tuner movements (see Fig. 10 bottom) but only poor agreement in  $\vec{V}$ , that therefore were neglected for the tuning process.

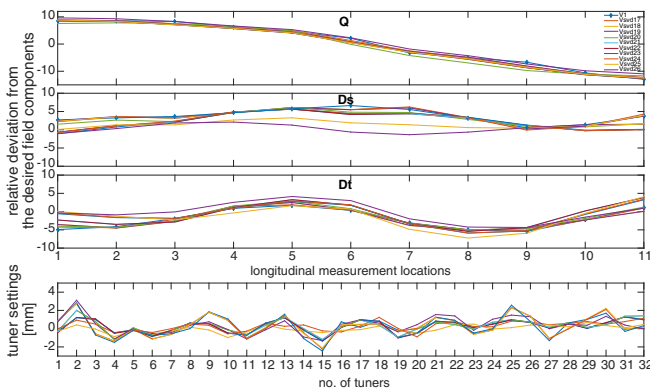


FIG. 10. The top three plots show several predictions for field compensation for Q, Ds, and Dt components separately. The bottom plot illustrates the corresponding tuner settings.

### C. Field tuning

After the reliability measurements the tuning process was started. Figure 11 shows the initial field distribution of the Q, Ds, and Dt component of the fully assembled RFQ. The purple crosses indicate the 11 measurement points along the length of the RFQ that were taken for the calculations of matrix  $\mathbf{M}$  described in Sec. IV B 1.

First, all tuners have been moved one by one by 3 mm inside the cavity. For each tuner movement a bead pull measurement was executed to obtain the influence of every single tuner on the longitudinal field distribution of all components at the locations indicated in Fig. 11 by crosses. Figure 12 shows all tuner influences on the different field components.

From these data the vector  $\vec{V}$  and the response matrix  $\mathbf{M}$ , as explained in Sec. IV B 1, were determined. After inversion of the matrix  $\mathbf{M}$  and manipulation of the singular values, 32 solutions for tuner settings were found as described in Sec. IV B 2. From comparison of  $\vec{V}$  with  $\vec{V}_{svdi}$  an optimum solution for tuner settings  $\vec{T}_{svd21}$  was

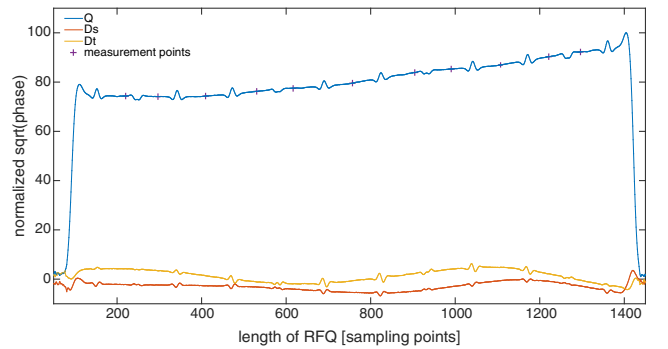


FIG. 11. The plot shows the relative longitudinal field distribution of the Q, Ds and Dt components before tuning. The longitudinal measurement locations are marked as crosses.

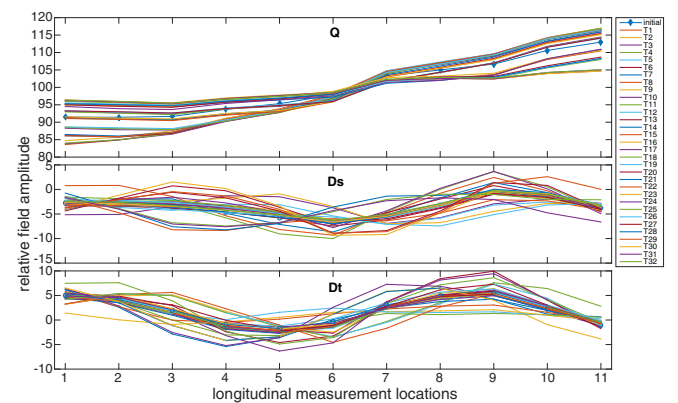


FIG. 12. The plot illustrates the change of the relative longitudinal field distributions of the Q, Ds, and Dt components by moving all 32 tuners one by one. The same normalization factor has been used for all curves.

found to start the tuning process. The predicted tuner displacements of  $\vec{T}_{svd21}$  were applied to the 32 tuners followed by bead pull measurements. From the new field distribution a new  $\vec{V}$  was calculated and by making use of the matrix again a new  $\vec{T}$  was computed and applied to the tuners.

This procedure of applying tuner corrections, measuring field and calculating new corrections was repeated four times. The change of the quadrupole and dipole components within the first four tuning iterations are presented in Figs. 13 and 14.

After four iterations the Q component was already well compensated, but there is almost no change on Ds and Dt noticeable from 3rd to 4th iteration as shown in Fig. 14. This means the solution has already converged and no significant change of the dipole components is expected any more.

At this point either all tuners have to be moved again to obtain a new matrix, which is very tedious work and brings the risk of introducing errors, or another solution from the

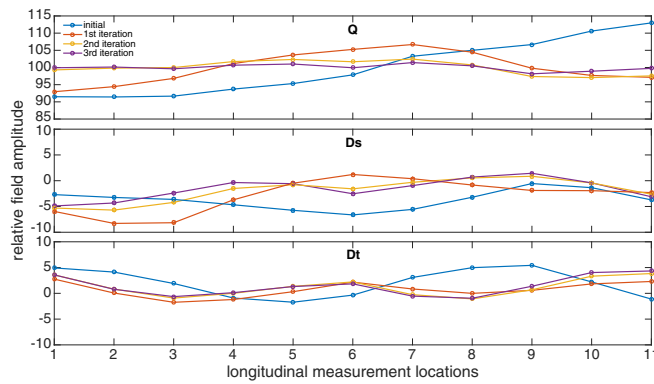


FIG. 13. The plot shows the change of the field distribution of the Q, Ds, and Dt components for the initial state as well as for the 1st, 2nd, and 3rd tuning iteration.

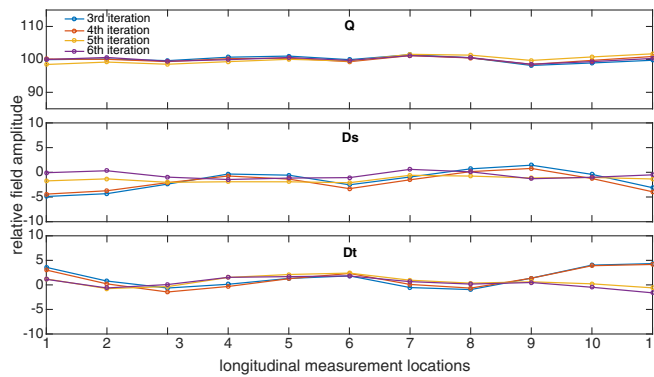


FIG. 14. The plot shows the change of the field distribution of the Q, Ds, and Dt components for the 3rd to the 6th tuning iteration.

already 32 obtained solutions can be used. The latter is explained in the following.

Figure 15 shows the predictions of the field compensation. The horizontal axis shows the longitudinal measurement points for the Q, Ds, and Dt components. On the vertical axis the relative deviation from the desired field components is depicted.

In this plot the dark blue line represents the initial field that needs to be compensated. The purple line is the prediction for the first tuning iteration and shows a very good agreement with the dark blue line for the quadrupole component. After four tuning iterations the field to be compensated is given by the red line. The prediction to compensate this, see line in light blue, shows a poor agreement with the red line in case of the Ds and Dt components. For this reason another solution from the 32 predictions was chosen. The prediction of the next tuning iteration using now  $\vec{V}_{svd18}$  is given by the yellow line. This shows an acceptable agreement for the quadrupole mode, which is anyway very well compensated already, but a much better agreement with the two dipolar components. After two more iterations, 5th and 6th iterations shown in Fig. 14, with  $\vec{V}_{svd18}$  the compensation of all modes was in a very acceptable range. All the field and frequency adjustment steps with the corresponding field errors is shown in Table III.

## D. Frequency tuning

### 1. Determination of the target frequency

Tuning of the frequency is not included in the field tuning algorithm. However in order to adjust the RFQ frequency to the operating frequency and simultaneously keeping the field distribution constant, all tuners have to be moved equally by the same amount of length to approach the target frequency of 749.48 MHz, a subharmonic of the

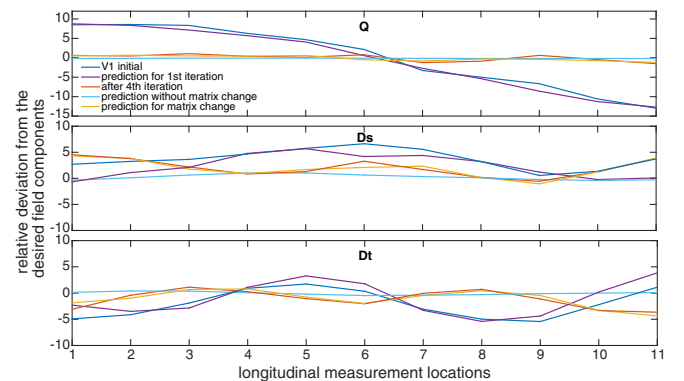


FIG. 15. The plot shows several so called predictions of how good a certain tuner setting solution compensates the longitudinal field errors from top to bottom for the Q, Ds, and Dt component. The yellow curve shows that a matrix change after 4th iteration is compensating both dipole components much better than without a matrix change.

TABLE III. Field and frequency tuning steps and tuner cutting in chronologic order.

Field Tuning	Frequency Tuning	Tuner Machining	Error Q	Error Ds	Error Dt	Comment
initial			$\pm 10.78\%$	$\pm 3.04\%$	$\pm 3.57\%$	
1			$\pm 6.87\%$	$\pm 4.75\%$	$\pm 2.25\%$	solution $T_{svd}21$
2			$\pm 2.69\%$	$\pm 3.28\%$	$\pm 2.46\%$	solution $T_{svd}21$
3			$\pm 1.63\%$	$\pm 3.16\%$	$\pm 2.64\%$	solution $T_{svd}21$
4			$\pm 1.33\%$	$\pm 2.60\%$	$\pm 2.80\%$	solution $T_{svd}21$
	1		$\pm 1.29\%$	$\pm 2.55\%$	$\pm 2.39\%$	all $T - 0.5\text{mm}$
5			$\pm 1.61\%$	$\pm 0.75\%$	$\pm 1.58\%$	solution $T_{svd}18$
6			$\pm 1.32\%$	$\pm 1.03\%$	$\pm 1.72\%$	solution $T_{svd}18$
	2		$\pm 1.10\%$	$\pm 1.15\%$	$\pm 1.63\%$	all $T - 0.2\text{mm}$
	3		$\pm 0.94\%$	$\pm 1.07\%$	$\pm 1.37\%$	all $T - 0.5\text{ mm}$
	4			no bead pull measurement		all $T - 0.2\text{ mm}$
	5		$\pm 1.07\%$	$\pm 1.05\%$	$\pm 1.57\%$	all $T - 0.03\text{ mm}$
	6		$\pm 1.02\%$	$\pm 0.80\%$	$\pm 1.65\%$	all $T - 0.02\text{ mm}$
		1	$\pm 1.38\%$	$\pm 1.07\%$	$\pm 1.72\%$	fixed with springs
		2	$\pm 1.04\%$	$\pm 1.04\%$	$\pm 1.71\%$	final copper gasket

LIGHT S-band cavities operating at 2997.92 GHz. Since 749.48 MHz is the RFQ frequency in vacuum and setting the cavity under vacuum was not possible with the tuner tooling attached, the frequency had to be scaled to be measured in dry nitrogen which was injected with a light flow during precise frequency adjustment. In addition the influence of the wire for bead pull measurements and the operation temperature of 24 °C was taken into account as well, leading to a target frequency of 749.2623 MHz.

## 2. Frequency adjustment

Figure 16 shows the frequency at the different tuning and frequency adjustment steps.

It shows also that the tuning iterations increase the frequency of the RFQ. In order to stay in a reasonable physical tuner range a first frequency adjustment was done after the fourth 4 field tuning iteration. Two more field

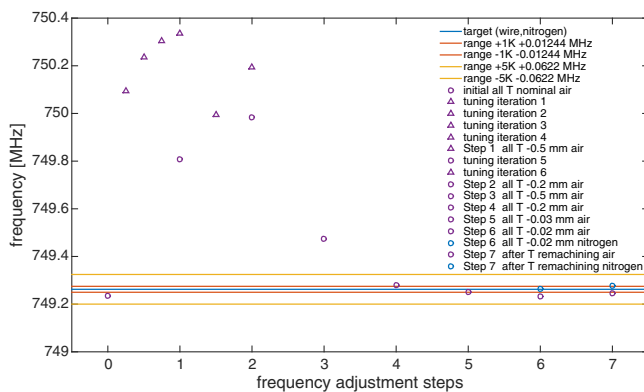


FIG. 16. The plot shows the different frequency adjustment steps that were made until the target frequency was approached. The horizontal lines mark the target, the preferable and acceptable frequency range.

tuning iterations increased the frequency further. Then the field errors were in an acceptable range and the tuners were moved all equally in order to adjust the frequency. After five frequency adjustment steps the target frequency was reached (step 6 in Fig. 16) and the tuners were cut to their proper individual length. After tuner machining and assembly (step 7) the frequency was unexpectedly too low. This is explained in more detail in the paragraph IV D 3. After a second tuner remachining and assembly the target frequency was set (step 8). After the proper frequency was set the field distribution was confirmed without significant changes, Fig. 17.

## 3. Tuner cutting

The tuners were premachined with an additional length of 11 mm. The penetration depth of the tuners was measured using a scaling on the screw-nut using the turns of the thread and additionally with a caliber from the

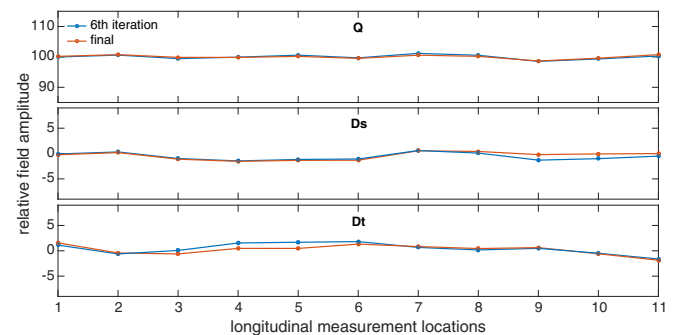


FIG. 17. The plot shows the field distribution of the Q, Ds, and Dt component for the last tuning iteration 6 and the final field distribution after frequency adjustment and final assembly of the tuners with copper gaskets.

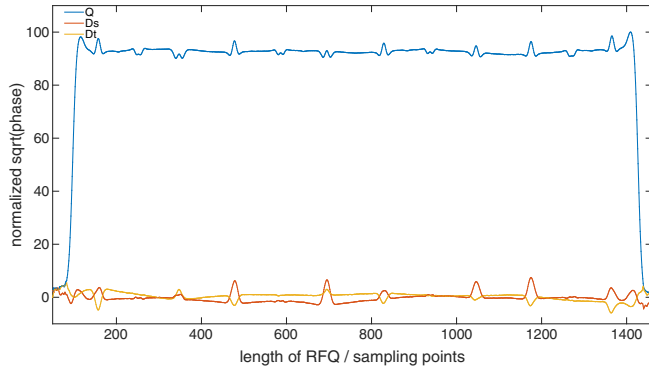


FIG. 18. The plot shows the detailed field distribution the of Q, Ds, and Dt components after field and frequency tuning. The horizontal axis shows the sampling points of the VNA instead of the longitudinal measurement location. This presentation allows to see the local field perturbations caused by the tuners.

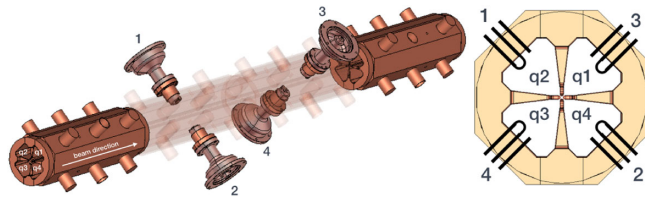


FIG. 19. The picture shows a 3D drawing of the RFQ with tuners, pumping ports, and power couplers (left) and a cross section of the RFQ indicating the numbering of the quadrants and the power couplers.

backside of the tuner flange to a reference surface at the tuner tooling. The agreement of both measurement methods was within a maximum error of  $\pm 0.06$  mm.

During field tuning each tuner was set to its individual penetration depth. This was measured and in order to insert them with their final length the tuners were remachined. After the cutting of the tuners to the determined length and assembly with the final copper gaskets, the frequency and field distribution was confirmed to be in the desired range. Frequency measurement in vacuum have given a frequency deviation of 0.00125 MHz above the target frequency. Figure 18 shows the bead pull measurement of the Q, Ds, Dt components after field and frequency tuning.

TABLE IV. Definitions for Q-factor calculations.

Parameter	Definition
$Q_{0_i}^*$	effective $Q_0$ that accounts for the losses to the other couplers <sup>a</sup> calculated from the S11 measurement of coupler $i$
$Q_{L_i}^*$	$Q_L$ calculated from the S11 measurement taken from coupler $i$
$Q_{ext_i}$	external Q-factor of couplers $i$ calculated from $Q_{0_i}^*$ and $Q_{L_i}^*$
$Q_{ext}$	total $Q_{ext}$ of all 4 power couplers
$Q_{0_i}$	$Q_0$ of the RFQ for each coupler measurement, they must be identical in case of no measurements errors
$Q_0$	mean value of all $Q_{0_i}$

<sup>a</sup>terminated by 50  $\Omega$  loads

## E. Power couplers/Q-values

For the determination of the different Q-values the S11 parameters of all power couplers have been measured as a function of frequency with a bandwidth of 1 MHz. Figure 19 shows the schematic power coupler configuration of the RFQ.

While one power coupler was measured the others were connected to 50  $\Omega$  attenuators. This setting is indicated with a \* at the Q-value. The definitions for the calculations are listed in Table IV. All measurements have been saved in the *Re/Im* format of a smith chart. Then  $Q_{0_i}^*$  and  $Q_{L_i}^*$  could be obtained from the data as described in Ref. [20].

From the measured  $Q_{0_i}^*$  and  $Q_{L_i}^*$ ,  $Q_{ext_i}$  were determined

$$Q_{ext_i} = \left( \frac{1}{Q_{L_i}^*} - \frac{1}{Q_{0_i}^*} \right)^{-1}. \quad (27)$$

Then the total  $Q_{ext}$  was calculated using

$$Q_{ext} = \left( \frac{1}{Q_{ext_1}} + \frac{1}{Q_{ext_2}} + \frac{1}{Q_{ext_3}} + \frac{1}{Q_{ext_4}} \right)^{-1} \quad (28)$$

to obtain  $Q_{0_i}$  with the following formula

$$Q_{0_i} = \left( \frac{1}{Q_{L_i}^*} - \frac{1}{Q_{ext_i}} \right)^{-1}. \quad (29)$$

The measured parameters are listed in Table V together with the design values for comparison.

## F. Antenna calibration

For the antenna calibration  $S_{21}$  parameters from all 4 power couplers to all 16 antennas have been measured at operating frequency. This data was used on the one hand to observe a possible change of longitudinal field distribution, for example due to transport, installation or during operation and on the other hand calculate the output power at the antennas at the nominal voltage of 67.6 kV.

### 1. Field distribution

In order to be able to observe a change of the field distributions the relative field levels at the locations of the

TABLE V. Comparison of the designed and measured quality factors.

Component	Design	Measurement
$Q_{0_1}$	6440	6492
$Q_{0_2}$	6440	6492
$Q_{0_3}$	6440	6355
$Q_{0_4}$	6440	6944
$Q_{\text{ext}_1}$	21900	26060
$Q_{\text{ext}_2}$	21900	27878
$Q_{\text{ext}_3}$	21900	27878
$Q_{\text{ext}_4}$	21900	21410
$Q_0$	6440	6570
$Q_{\text{ext}}$	5475	6377
Coupling $\beta$	1.18	1.03

pickup antennas from bead pull measurements have been compared to the  $S_{21}$  measurements from all power couplers to all antennas.

Each  $S_{21}$  measurements is a function of the external Q of the coupler and of the antenna

$$S_{21}^{C_1-A_1}(Q_{\text{ext}}^{C_1}, Q_{\text{ext}}^{A_1}) \quad (30)$$

which depends on the coupling and the field level at the location of the coupler and antenna

$$S_{21}^{C_1-A_1}((F_{C_1}; \beta_{C_1}); (F_{A_1}; \beta_{A_1})). \quad (31)$$

This means that the  $S_{21}$  measurements are proportional to a function of the field and the coupling at every antenna

$$S_{21} \propto F \cdot \beta. \quad (32)$$

Since only the relative field distribution is of interest each measurement can be normalized to a measurement of any other antenna.  $S_{21}^{C_1-A_i}$  is the  $S_{21}$  measurement from coupler 1 to the  $i$ -th antenna that is normalized to the measurement from coupler 1 to antenna 1.

$$\frac{S_{21}^{C_1-A_i}}{S_{21}^{C_1-A_1}} \propto \frac{f(F_{A_i} \cdot \beta_{A_i})}{f(F_{A_1} \cdot \beta_{A_1})}. \quad (33)$$

Since the coupling is not changed  $\beta_i/\beta_1$  is constant and the ratio in Eq. (33) only depends on a possible change of field. By dividing the magnitude of the  $S_{21}$  measurements of one power coupler to all antennas normalized to antenna 1 by the field level at the location of the antennas obtained from bead pull measurements also normalized to the field value at the location of antenna 1, one receives curves (shown in Fig. 20) that should be equal for all 4 measurements for each power coupler. This is a characteristic curve for the antenna settings for this RFQ. A change of field would result in a displacement of all four coupler to antenna measurements compared to the situation before. Figure 20

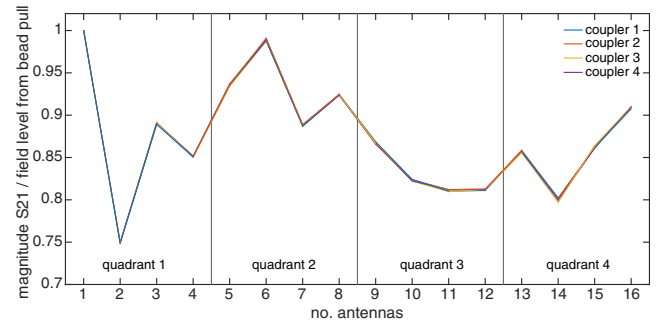


FIG. 20. The plot shows the characteristic curve of the antenna calibration. The different quadrants are separated by vertical lines.

shows the measurements at CERN before the transport of the RFQ.

The plot in Fig. 20 shows a good agreement of all curves. Slight deviations are related to measurement errors. A displacement of a new measurements of all four curves to the four curves measured before would be a clear indication of a field change.

## 2. Power level at the antenna output

Parameter definitions for the calculations in this paragraph are listed in Table VI.

Table VII lists the parameters used for the following calculations.

TABLE VI. Parameter definitions.

Parameter	Definition
$Q_0^{\text{sim}}$	$Q_0$ design value
$P_0^{\text{sim}}$	design value of nominal power to obtain nominal voltage of 67.6 kV
$Q_0^{\text{meas}}$	measured $Q_0$ value
$S_{21}^{C_i A_j}$	magnitudes of $S_{21}$ -measurement in dB from coupler $i = 1, \dots, 4$ to antenna $j = 1, \dots, 16$
$W_0$	energy stored in the RFQ
$\omega$	$2 \cdot \pi \cdot f$
$f$	nominal frequency of the RFQ

TABLE VII. Parameters used for calculations.

Parameter	Value	Unit
Frequency	749.48	MHz
$Q_0^{\text{sim}}$	6440	
$P_0^{\text{sim}}$	340	kW
$Q_0^{\text{meas}}$	6570	
$S_{21}^{C1A1}$	-59.49	dB
$S_{21}^{C2A1}$	-59.67	dB
$S_{21}^{C3A1}$	-60.04	dB
$S_{21}^{C4A1}$	-58.71	dB

The design value of the energy stored in the RFQ at the nominal voltage of 67.6 kV is given by

$$W_0 = \frac{Q_0^{\text{sim}} \cdot P_0^{\text{sim}}}{\omega} = 0.465J. \quad (34)$$

The power needed to achieve the nominal stored energy for the measured quality factor is given by

$$P_L = \frac{W_0 \cdot \omega}{Q_{\text{meas}}} = 334 \text{ kW}. \quad (35)$$

This agrees well with the design power of 340 kW. Then the power expected to be measured at the pickup antenna for the total input power for all 4 couplers of 334 kW is calculated by

$$P_0^{A1} = S_{21}^2 \cdot P_L = 1.51 \text{ W} \quad (36)$$

with

$$S_{21}^2 = (S_{21}^{C1A1})^2 + (S_{21}^{C2A1})^2 + (S_{21}^{C3A1})^2 + (S_{21}^{C4A1})^2. \quad (37)$$

This shows also a good agreement with the design value of 1.4 W.

### ACKNOWLEDGMENTS

We wish to acknowledge the support of Sebastien Calvo, Yves Cuvet, Veliko Dimov, Alessandra Lombardi, Serge Mathot, Eric Montesinos, Carlo Rossi, Maurizio Vretenar for their great contribution to the successful tuning of the RFQ.

- 
- [1] LIGHT, Product overview, <http://www.avopl.com/Our-LIGHT-system/Product-overview>.
- [2] M. Vretenar *et al.*, High-Frequency compact RFQs for medical and industrial applications, in *Proc. LINAC 2016, East Lansing, Michigan, USA, 2016* (JACoW, Geneva, Switzerland, 2016).
- [3] A. Lombardi *et al.*, Beam dynamics in a high frequency RFQ, in *Proc. IPAC 2015, Richmond, USA, 2015* (JACoW, Geneva, Switzerland, 2015), p. 2408.
- [4] M. Vretenar *et al.*, A compact high-frequency RFQ for medical applications, in *Proc. LINAC 2014, Geneva, Switzerland, 2014* (JACoW, Geneva, Switzerland, 2014), p. 935.
- [5] S. O. Schriber, Analog analysis of  $\pi$ -mode structures: Results and implications, *Phys. Rev. ST Accel. Beams* **4**, 122001 (2001).
- [6] M. R. Khalvati and S. Ramberger, Straightforward and accurate technique for post-coupler stabilization in drift tube linac structures, *Phys. Rev. Accel. Beams* **19**, 042001 (2016).
- [7] F. Grespan, , Equivalent circuit for postcoupler stabilization in a drift tube linac, *Phys. Rev. ST Accel. Beams* **15**, 010101 (2012).
- [8] A. Palmieri *et al.*, Perturbation analysis on a four-vane RFQ, in *Proceedings of the International Particle Accelerator Conference, Kyoto, Japan* (ICR, Kyoto, 2010), p. 606.
- [9] A. France and F. Simones, Theoretical analysis of a real-life RFQ using a 4-WIRE line model and the theory of differential operators, in *Proceedings of the 8th European Particle Accelerator Conference, Paris, 2002* (EPS-IGA and CERN, Geneva, 2002), p. 957.
- [10] C. Y. Tan, J. S. Schmidt, and A. Schempp, Simple lumped circuit model applied to field flatness tuning of four-rod radio frequency quadrupoles, *Phys. Rev. ST Accel. Beams* **17**, 012002 (2014).
- [11] G. V. Lamanna *et al.*, Field tuning of the TRASCO RFQ, in *Proceedings of the 8th European Particle Accelerator Conference, Paris, 2002* (EPS-IGA and CERN, Geneva, 2002), p. 924.
- [12] L. Young, Tuning and stabilization of RFQ's, in *Proc. LINAC 1990, Albuquerque, New Mexico, USA, 1990* (1990), p. 530.
- [13] O. Piquet *et al.*, RF tuning of the LINAC4 RFQ, in *Proceedings of the 4th International Particle Accelerator Conference, IPAC-2013, Shanghai, China, 2013* (JACoW, Shanghai, China, 2013), p. 3761.
- [14] A. Pisent *et al.*, The TRASCO-SPES RFQ, in *Proceedings of LINAC 2004, Lübeck, Germany, 2004* (JACoW, 2004) pp. 69–71.
- [15] A. C. France *et al.*, RF Design and Tuning of LINAC4 RFQ, in *Proc. RUPAC 2012, Saint-Petersburg, Russia, 2012* (2012) pp. 448–450.
- [16] C. Rossi *et al.*, Progress in the Fabrication of the RFQ Accelerator for the CERN LINAC4, in *Proceedings of the 25th International Linear Accelerator Conference, LINAC-2010, Tsukuba, Japan* (KEK, Tsukuba, Japan, 2010), p. 497.
- [17] B. Koubek, A. Grudiev, Y. Cuvet, C. Rossi, and M. Timmins, Tuning of the CERN 750 MHz RFQ for medical applications, in *28th Linear Accelerator Conference (LINAC'16), East Lansing, MI, USA* (JACoW, Geneva, Switzerland, 2017), p. 763.
- [18] T. P. Wangler, *RF Linear Accelerators* (WILEY-VCH Verlag GmbH & Co. KGaA, Weinheim, 2008).
- [19] G. Golub and W. Kahan, Calculating the singular values and pseudo-inverse of a matrix, *J. Soc. Ind. Appl. Math. B Numer. Anal.* **2**, 205 (1965).
- [20] F. Caspers, RF engineering basic concepts: the Smith chart, in *Proc. CAS—CERN Accelerator School: RF for Accelerators 2011, Denmark, Ebeltoft, 2010*, edited by R. Bailey (CERN, 2011), p. 95.